THE FASEB JOURNAL • RESEARCH • www.fasebj.org

Induced Cre-mediated knockdown of Brca1 in skeletal muscle reduces mitochondrial respiration and prevents glucose intolerance in adult mice on a high-fat diet

Kathryn C. Jackson,* Michael D. Tarpey,† Ana P. Valencia,* Melissa R. Iñigo,*,† Stephen J. Pratt,‡ Daniel J. Patteson,† Joseph M. McClung,†,§ Richard M. Lovering,‡ David M. Thomson,¶ and Espen E. Spangenburg*,†,§,1

*Department of Kinesiology, School of Public Health, University of Maryland, College Park, Maryland, USA; †Department of Physiology, Brody School of Medicine, and §East Carolina Diabetes and Obesity Institute, East Carolina University, Greenville, North Carolina, USA; ‡Department of Orthopaedics, School of Medicine, University of Maryland, Baltimore, Maryland, USA; and ¶Department of Physiology and Developmental Biology, Brigham Young University, Provo, Utah, USA

ABSTRACT: The breast cancer type 1 susceptibility protein (Brca1) is a regulator of DNA repair in mammary gland cells; however, recent cell culture evidence suggests that Brca1 influences other processes, including those in nonmammary cells. In this study, we sought to determine whether Brca1 is necessary for metabolic regulation of skeletal muscle using a novel *in vivo* mouse model. We developed an inducible skeletal muscle-specific Brca1-knockout (BRCA1KO^{smi}) model to test whether Brca1 expression is necessary for maintenance of metabolic function of skeletal muscle when exposed to a high-fat diet (HFD). Our data demonstrated that deletion of Brca1 prevented HFD-induced alterations in glucose and insulin tolerance. Irrespective of diet, BRCA1KO^{smi} mice exhibited significantly lower ADP-stimulated complex I mitochondrial respiration rates compared to age-matched wild-type (WT) mice. The data show that Brca1 has the ability to localize to the mitochondria in skeletal muscle and that BRCA1KO^{smi} mice exhibit higher whole-body CO_2 production, respiratory exchange ratio, and energy expenditure, compared with the WT mice. Our results demonstrate that loss of Brca1 in skeletal muscle leads to dysregulated metabolic function, characterized by decreased mitochondrial respiration. Thus, any condition that results in loss of Brca1 function could induce metabolic imbalance in skeletal muscle.—Jackson, K. C., Tarpey, M. D., Valencia, A. P., Iñigo, M. R., Pratt, S. J., Patteson, D. J., McClung, J. M., Lovering, R. M., Thomson, D. M., Spangenburg, E. E. Induced Cre-mediated knockdown of Brca1 in skeletal muscle reduces mitochondrial respiration and prevents glucose intolerance in adult mice on a high-fat diet. FASEB J. 32, 3070–3084 (2018). www.fasebj.org

KEY WORDS: metabolism · disease · breast · cancer

Breast cancer 1, early-onset gene (*BRCA1* in humans; *Brca1* in mice) is a tumor-suppressor gene, whose protein product, termed breast cancer type 1 susceptibility protein (Brca1), is normally expressed in several cell types. Specific single-nucleotide polymorphisms in *BRCA1* are strongly linked to an increased risk of breast cancer development. Brca1 plays a critical role in DNA repair; thus, mutations in the gene that lead to loss of protein function can result in accumulation of damaged DNA within the cell (1). Despite its expression in many tissues, most work concerning Brca1 has been largely restricted to breast tissue. However, recent studies have demonstrated that Brca1 plays a critical role in vascular and neuronal tissues, suggesting that Brca1 plays a much larger physiologic role than previously identified (2–4).

We recently demonstrated that Brca1 is expressed in skeletal muscle and is a critical regulator of metabolic function in cultured human myotubes (5). Specifically, we found that *in vitro* knockdown of Brca1 expression resulted in reduced mitochondrial O_2 consumption in these cells (5). Others have shown that overexpression of Brca1 in cultured MCF7 cells, a breast cancer cell line, increased oxidative gene expression, whereas loss of Brca1 expression increased glycolytic gene expression (6). In addition,

ABBREVIATIONS: Brca1, breast cancer type 1 susceptibility protein; BRCA1KO^{smi}, inducible skeletal muscle-specific Brca1 knockout; CD, control diet; Co-A, coenzyme A; Drp, dynamin-related protein; FDB, flexor digitorum brevis; GLUT, glucose transporter; GTT, glucose tolerance test; HFD, high-fat diet; HK, hexokinase; HSA, human skeleton actin; IMLC, intramuscular lipid content; IP, intraperitoneal; ITT, insulin tolerance test; KO, knockout; LDH, lactate dehydrogenase; mER-Cre-mER, tamoxifen-inducible *Cre* recombinase; PFK, phosphofructokinase; RER, respiratory exchange ratio; V_{CO_2}, volume of CO_2; Veh, vehicle; V_{O_2}, volume of O_2; WT, wild type; YFP, yellow fluorescent protein

[1] Correspondence: East Carolina Diabetes and Obesity Institute, Department of Physiology, Brody School of Medicine, East Carolina University, 115 Heart Dr., Greenville, NC 27834. E-mail: spangenburge14@ecu.edu

doi: 10.1096/fj.201700464R

0892-6638/18/0032-3070 © FASEB

deletion of Brca1 expression in vascular cells results in reduced catabolic breakdown of free fatty acids (6, 7). The published data suggest that manipulation of Brca1 expression influences the metabolic phenotype of cultured cells and potentially the ability of the cells to respond to conditions of nutrient overload.

Recent data in cultured cells (endothelial and fibroblast) found that Brca1 was localized to the mitochondria (8, 9), which is surprising because Brca1 lacks a traditional mitochondrial localization sequence. In these cells, Brca1 was found throughout the mitochondrial matrix, suggesting colocalization with the mitochondrial DNA (8). These studies suggest that manipulation of Brca1 expression affects mitochondrial function of cultured cells. To the best of our knowledge, no studies have considered an *in vivo* metabolic role for Brca1 in skeletal muscle.

The purpose of this study was to determine whether Brca1 expression in skeletal muscle is critical to the regulation of metabolic function *in vivo*. Using a novel inducible skeletal muscle–specific Brca1 knockout (KO) mouse, we hypothesized that a reduction of Brca1 protein content in skeletal muscle would increase the development of metabolic dysfunction in response to nutrient overload induced by a high-fat diet (HFD). We found that decreases in Brca1 expression led to a significant reduction in mitochondrial respiration and improved glucose tolerance after HFD. As in other cell types, in skeletal muscle we observed Brca1 colocalization to the mitochondria, supporting a potential novel role for Brca1 in muscle mitochondrial function. Overall, these findings provide critical evidence that Brca1 expression is essential for maintaining the metabolic phenotype of skeletal muscle.

MATERIALS AND METHODS

Generation of human skeleton actin-Cre^{+} Brca1$^{fl/fl}$ mouse

Female mice with flox sites flanking exon 11 of the Brca1 gene (referred to as Brca1$^{fl/fl}$, obtained from the National Cancer Institute Mouse Repository, Bethesda, MD, USA) were bred with male mice containing a skeletal muscle tissue–specific tamoxifen-inducible Cre recombinase (mER-Cre-mER) (kind gift of Dr. Karyn Esser, University of Florida, Gainesville, FL, USA, and Dr. John J. McCarthy, University of Kentucky, Lexington, KY, USA) (**Fig. 1**). The breeding scheme generated offspring human skeleton actin (HSA)-mER-Cre-mER^{+}-Brca1$^{fl/-}$, which were bred to female Brca1$^{fl/fl}$, resulting in HSA-mER-Cre-mER^{+}-Brca1$^{fl/fl}$ mice. HSA-mER-Cre-mER^{+}-Brca1$^{fl/fl}$ mice were then backcrossed for 8–9 generations before use, with the background strain being C57/Bl6NJ. The University of Maryland and East Carolina University Institutional Animal Care and Use Committee Review Boards approved all aspects involving the described animal research. In addition, all guidelines from the *Guide for the Care and Use of Laboratory Animals* [National Institutes of Health (NIH), Bethesda, MD, USA] were followed.

Animal genotyping

All animals were genotyped based on the presence of HSA-Cre and homozygote Brca1 flox expression using genomic DNA. Primer sets for Mer-Cre-Mer F-5′-GGCATGGTGGAGATCTTTGA-3′ and R-5′-CGACCGGCAAACGGACAGAAGC-3′ were used to screen for HSA-mER-Cre-mER^{+} animals (10). Concurrently, all animals were also genotyped for Brca1 flox using primer sets B004-5′-CTGGGTAGTTTGTAAGCATGC-3′ and B005-5′-CAATAAACTGCTGGTCTCAGG-3′ where the Brca1 flox amplicon is ~500 bp and the wild-type (WT) is ~450 bp.

Brca1 recombination DNA analysis

Cre-mediated recombination was confirmed through PCR analysis of genomic DNA with a DNA Isolation Kit (Qiagen, Germantown, MD, USA). Specifically, primer Brca1 Flox-A-5′-CTGGGTAGTTTGTAAGCATGC-3′ and primer Brca1 Flox-E-5′-CTGCGAGCAGTCTTCAGAAAG-3′ (**Fig. 2*A***) were used to generate an amplicon that was ~621 bp in length, which indicated recombination and removal of the flox region of Brca1, as has been described (11). In contrast, failure to detect an amplicon indicates no active recombination of the flox sites. No differences were found in the amount of mER-Cre-mER protein across sexes in the mouse model (Fig. 2*B*). The recombination events were consistent with previously described results using the HSA-driven mER-Cre-mER mouse (10). Exon 11 is the largest exon in *BRCA1*, with previous work demonstrating that excision of exon 11 results in loss of full-length Brca1 function (11).

Experimental approach

Ten-week-old HSA-mER-Cre-mER^{+}-Brca1$^{fl/fl}$ male and female mice were injected intraperitoneally (IP) with 2 mg/d tamoxifen or vehicle solution for 5 consecutive days. Preliminary experiments found that flox recombination was detectable within days

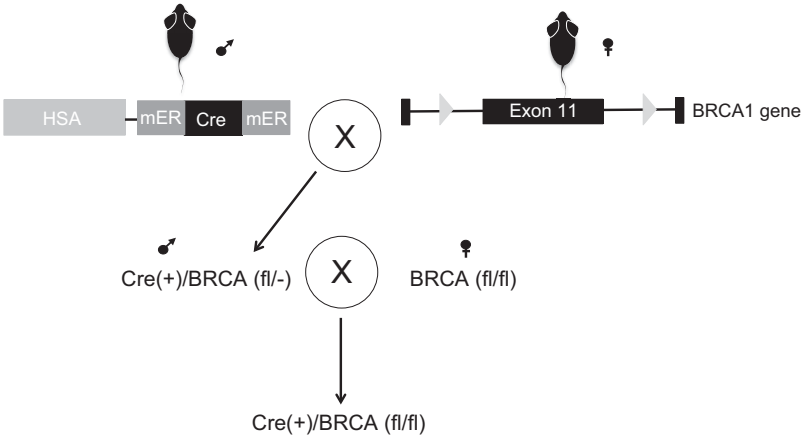

Figure 1. Creation of a BRCA1KO^{smi} mouse. HSA-mER-Cre-mER mice (10) were crossed with *BRCA1$^{fl/fl}$* mice, which have flox sites flanking exon 11 within the BRCA1 gene (11). Exon 11 in the *BRCA1* is the largest exon in the *BRCA1* gene (~3400 bp) accounting for 60% of coding sequence. Male mice positive for Cre and BRCA1$^{fl/fl}$ were mated to female mice positive for BRCA1$^{fl/fl}$, but negative for Cre. Only offspring that were Cre^{+} were used in these studies. Ten-week-old HSA-Cre^{+} BRCA1 Flox$^{+/+}$ male and female mice were injected with 2 mg/d tamoxifen or vehicle solution for 5 consecutive days. In all figures, BRCA1KO^{smi} mice are referred to as KO and vehicle-injected mice as WT.

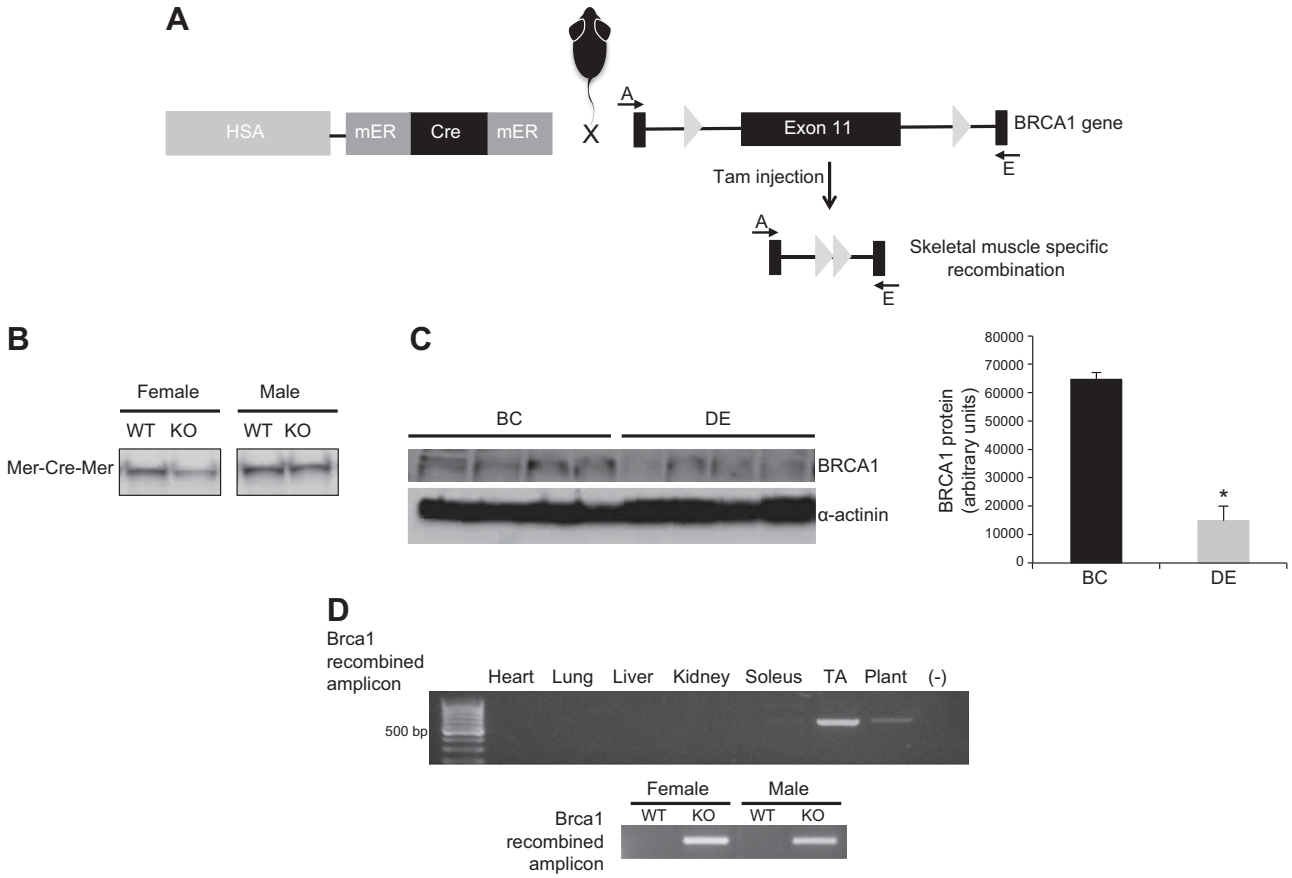

Figure 2. Induction of flox recombination of the *BRCA1* gene specifically in skeletal muscle. *A*) Injection of tamoxifen resulted in the deletion of exon 11 of *BRCA1*. *B*) The mER-Cre-mER transgene was expressed in gastrocnemius muscle of male and female mice after mice were crossed with the BRCA1$^{fl/fl}$ strain. *C*) Injection of tamoxifen for 5 d resulted in the recombination of the flox sites, deleting exon 11. A PCR strategy was used, where primers A—E were aligned to either side of exon 11 outside of the flox sites. Because of the large size of exon 11, the PCR failed to produce a product without successful recombination of the flox sites. Successful recombination of the flox sites resulted in a PCR product of 621 bp. Tissue was collected from animals at 3 wk after injection, and recombination was found to occur only in skeletal muscle, with no recombination occurring in the heart or any nonstriated muscle. −, refers to the negative control. Recombination occurred in male and female mice with similar fidelity. *D*) Decreases in Brca1 protein were detected in the gastrocnemius muscle of the tamoxifen-injected compared to Veh-injected mice. We did not see complete loss of BRCA1 content, which was likely because signal was derived from other cell types, such as the intraskeletal muscle vasculature. BRCA1 expression is also found in vascular and neuronal cells (20). Means ± SEM. *$P < 0.05$.

after completing the 5-d injection protocol; however, to ensure that no off-target effects occurred, animals underwent a 14 d washout period before assignment to experimental groups. In the figures, animals receiving tamoxifen injections are referred to as KO mice, and mice receiving vehicle injections are referred to as WT mice. Upon completing the 14-d washout period, animals were randomly assigned to receive either a control diet (low-fat) (CD; 10% kcal fat; D12450K) (KO-CD; WT-CD) or a HFD (45% kcal fat; D12451) (WT-HFD; KO+HFD) (Research Diets, New Brunswick, NJ, USA) for a duration of 12 wk. Food intake and body weight were recorded during the 11 wk of feeding. Upon completing these measures, mice were euthanized at wk 12, and tissues were either processed or flash frozen and stored at −80°C. We also performed control experiments in a parallel cohort to account for any nonspecific effects of tamoxifen or vehicle delivery by injecting HSA- mER-Cre-mER^{+} in the same manner as described above, with the tissue captured in the same fashion.

Glucose–insulin tolerance testing

For glucose tolerance testing (GTT), animals from each group (n = 8/group) were left unfed overnight in cages containing hardwood bedding before GTT, whereas for insulin tolerance tests (ITTs), animals retained access to food. Before injecting glucose or insulin on the day of the test, fed (GTT) and unfed (ITT) basal blood glucose levels were measured. For GTTs, animals were injected IP with 0.001 g glucose/g body weight. For ITTs, animals were injected with recombinant insulin dissolved in sterile PBS and with 1.0 U insulin (Humalin; Eli Lilly, Indianapolis, IN, USA) per 1 kg body weight. Blood glucose levels were measured with a glucometer (AlphaTrak; Abbott, Chicago, IL, USA) before injection (0) and at 30, 60, 90, and 120 min after glucose or insulin injection. A 72-h washout period occurred between GTT and ITT procedures.

Mitochondrial respiration measures

Skeletal muscle mitochondria were isolated from animals from each group (n = 6–8/group) according to previously described methods with slight modifications (12). Quadriceps muscles were collected and immediately placed in ice-cold PBS supplemented with 10 mM EDTA. Connective tissue was removed, and muscles were minced with scissors during incubation on ice in PBS/EDTA 0.05% trypsin for 30 min. The muscles were

then homogenized with a 30 ml glass/Teflon potter Elvehjem Tissue Grinder (Omni International, Kennesaw, GA, USA) in isolation buffer 1 containing 67 mM mannitol, 50 mM Tris/HCl, 1 mM EDTA, and 1 mg/ml bovine serum albumin (pH 7.4). The homogenate was transferred to a conical tube and centrifuged at 700 *g* for 10 min at 4°C. The supernatant was transferred and centrifuged at 8000 *g* for 10 min at 4°C. The pellet was resuspended in isolation buffer 2, containing 300 mM mannitol, 10 mM Tris/HCl, and 3 mM EGTA/Tris, then centrifuged at 8000 *g* for 10 min at 4°C. The resulting supernatant was discarded. The pellet was then resuspended in 50 μl of respiration buffer [125 mM KCl, 2 mM K_2PO_4, 10 mM 4-(2-hydroxyethyl)-1-piperazineethanesulfonic acid (HEPES), 1 mM MgCl, 0.1 mM EGTA, and 1% bovine serum albumin] for mitochondrial respiration measurements. The protein concentration of the pellet was determined using the Pierce BCA Protein Assay (Thermo Fisher Scientific, Waltham, MA, USA).

Mitochondrial respiration was measured (Hanstech, Norfolk, United Kingdom) as has been previously described (12). Freshly isolated mitochondria from each group were placed in the calibrated electrode chamber containing 500 μl respiration buffer. Basal respiration was induced with addition of 0.5 mM glutamate/0.025 mM malate to the respiration buffer. ADP stimulated respiration was induced with the delivery of 300 μM ADP to the chamber. Where possible, each sample was run at least in triplicate. Oxygen consumption rates were then normalized to mitochondrial protein content.

Intramuscular lipid content

To determine intramuscular lipid content (IMLC), lipid droplets were visualized and quantified by using Bodipy (493/503) (Thermo Fisher Scientific) staining of the tibialis anterior (TA) muscles from all groups (n = 6/group), as described by our group (13).

Immunoblot analysis

Immunoblot analysis with whole-muscle homogenate protein was performed (5, 14). Membranes were probed with an antibody specific to BRCA1 (I-20, rabbit polyclonal, sc-646; 1:200; Santa Cruz Biotechnology, Dallas, TX, USA), total oxphos (ab110413, mouse monoclonal, 1:1000; Abcam, Boston, MA, USA), and α-actinin (EA-53, A7732, mouse monoclonal, 1:5000; MilliporeSigma, Billerica, MA, USA).

Mouse malonyl CoA measures

Malonyl coenzyme A (CoA) measures were performed on the plantaris muscles (5).

Electron microscopy imaging of skeletal muscle

The deep (red) portions of the gastrocnemius muscles were removed, cut into 1 mm^3 cubes and incubated fixed overnight with 2.5% (v/v) glutaraldehyde, 2.0% (v/v) paraformaldehyde in 0.1 M sodium cacodylate buffer (pH 7.4), overnight at 4°C. Samples were sectioned for electron microscopy at ~90 nm, and viewed with a 201 microscope (Phillips, Eindhoven, The Netherlands) similar to the published method (15).

BRCA1 localization measure

cDNA specific for BRCA1 harboring a yellow fluorescent protein (YFP) tag was electroporated into the flexor digitorum brevis (FDB) muscle of young male mice (16). Full length BRCA1-YFP plasmid was a kind gift of Dr. B. Henderson (Westmead Institute for Cancer Research, Sydney, NSW, Australia (17). After 1 wk, the muscle was removed from mice under general anesthesia, and single muscle fibers were isolated. The isolated FDB fibers were incubated with MitoTracker DeepRed and NucBlue (Thermo Fisher Scientific) for 30 min. The fibers were carefully washed with sterile Krebs-Ringer Buffer and immediately imaged with a Fluoview FV1000 Confocal Microscope (Olympus, Center Valley, PA, USA). Images were captured at ×60 magnification, ensuring the Nyquist spatial sampling was appropriate, and colocalization was assessed with ImageJ software (NIH) according to recommended procedures (18). The YFP localization varied across the fiber, and Mander's coefficient was therefore calculated to determine spatial localization of BRCA-YFP and MitoTracker or DAPI.

Assessment of whole body energy metabolism

The TSE LabMaster System (TSE System, Chesterfield, MO, USA) was used to determine whole-body volume of O_2 (V_{O_2}) consumption and volume of CO_2 (V_{CO_2}) production, respiratory exchange ratio (RER), and energy expenditure. Data were captured over a 3-d period after 2 d of acclimation. Data represent the average over the 3 d.

Acute exercise tolerance bout

An endurance exercise test was performed for each of the 4 groups of mice. The endurance test consisted of a 3 d treadmill acclimation period where animals were placed on the treadmill with the electrical shock grid in the rear turned on for 3 min and then the treadmill speed was increased to 11 m/min for 5 min each day (14). Mice rested for 1 d before the exercise test. On the day of the test, mice began running at 11 m/min at a 5% incline, and speed was increased 2 m/min every 5 min, until the maximum speed was reached—determined by each animal's ability to remain on the treadmill for a minimum of 20-s bouts. Failure was classified as animals remaining on the shock grid for more than 15 continuous seconds. Exercise distance and exercise duration were recorded for each animal, to assess exercise tolerance in each group of animals.

Statistical analysis

All data are means ± SEM. Statistical analysis was conducted with 2-way ANOVA with *post hoc* tests (Student-Newman Keuls) or a Student's t test, as appropriate. For confocal imaging experiments, we used Mander's coefficient calculations to determine the degree of spatial overlap between the YFP signal from BRCA1 and Mitotracker DS or NucBlue signal (Thermo Fisher Scientific). Mander's coefficient was used to determine the amount of fluorescence in colocalizing pixels for each channel. Statistical significance was set at $P \leq 0.05$.

RESULTS

Mouse model

Measurements of genomic DNA demonstrated that exon 11 of the *BRCA1* gene was efficiently deleted in skeletal muscle of tamoxifen-injected *vs.* vehicle-injected mice (Fig. 2*C, D*). Further, the recombination event was specific to skeletal muscle, because we did not find any evidence of recombination occurring in nonskeletal muscle tissues, nor did we find recombination occurring in vehicle-injected mice (Fig. 2*C*). Tamoxifen-induced flox recombination of

the *BRCA1* was equally efficient in both sexes of mice. The recombination event resulted in a significant reduction (78%) in Brca1 protein content of the gastrocnemius muscle (Fig. 2*D*), which is similar to what has been found in other conditional KO approaches. Complete loss of protein content is rarely found in induced conditional KO models, since skeletal muscle (19) contains several different cell types (*i.e.*, neurons, fibroblasts, endothelial cells, and smooth muscle), all of which are reported to express Brca1 (20). Thus, our data confirm that Brca1 content was significantly reduced, but likely knocked out in skeletal muscle after tamoxifen injections compared to Veh injections and support our model as an inducible skeletal muscle–specific BRCA1KO^{smi} mouse.

Body weight, food consumption, organ mass

Body weight significantly increased in all groups over the course of the study; however, the WT mice fed an HFD gained significantly more weight after week 6 compared with all other groups (**Fig. 3**). The BRCA1KO^{smi} mice consumed significantly more food per day regardless of diet when compared with the WT group (**Table 1**). No differences were detected in heart, liver, or skeletal muscle mass (**Fig. 4*A*–*C***) when comparing the WT and KO mice, regardless of diet. Fat pad mass of HFD-fed KO mice was not significantly different from those of the WT-HFD (P = 0.0809) or KO-CD (P = 0.0687) groups, although WT mice fed a 12 wk HFD exhibited significantly higher visceral fat mass compared to WT-CD mice. (Fig. 4*D*). Finally, in a parallel cohort of age-matched HSA-mER-Cre-mER mice that were injected with the tamoxifen protocol described above, we found no differences in body weight, food consumption, and organ mass compared to vehicle-injected mice (data not shown).

Glucose tolerance and insulin responses

WT mice exposed to an HFD for 12 wk exhibited significantly higher glucose responses at all time points tested after an IP glucose load compared with all other groups across all the time points tested (**Fig. 5*A***). No differences in basal glucose levels were detected across groups. Using area under the curve calculations, we found that the WT-HFD group exhibited significantly higher responses compared with the other groups (Fig. 5B). Consuming an HFD did not affect glucose tolerance in the BRCA1KO^{smi} mice. Using an ITT, the WT-HFD group was found to be the least responsive to insulin injection compared with all other groups (**Fig. 6*A***). Calculation of the slope from 0 to 30 min after insulin injection demonstrated a reduced insulin response in the WT-HFD group *vs.* all other groups (Fig. 6*B*). Response to the insulin injection resulted in a main effect of genotype at 120 min after insulin injection, where blood glucose levels were elevated in WT *vs.* BRCA1KO^{smi} mice (Fig. 6A). At 30 and 120 min after insulin injection, blood glucose levels for both WT-CD and BRCA1KO^{smi}-HFD mice were lower than in WT-HFD mice (Fig. 6*A*).

Skeletal muscle from BRCA1KO^{smi} does not exhibit alterations in glycolytic enzyme protein content compared to that in age-matched WT animals

Based on the changes found in glucose tolerance and insulin responses in BRCA1KO^{smi}, we assessed protein content of glucose transporter (GLUT)-4 and key glycolytic enzymes including hexokinase (HK)-II, phosphofructokinase (PFK), and lactate dehydrogenase (LDH) (**Fig. 7**). We found no significant differences in GLUT4 content between the BRCA1KO^{smi} and WT mice, nor did we find an influence of diet on GLUT4 (Fig. 7*A*). We found no effect of genotype or diet on skeletal muscle HKII protein content (Fig. 7*B*). In contrast, with PFK we found a significant main effect of diet on PFK protein content in both the BRCA1KO^{smi} and WT mice, whereas we did not find an effect of genotype (P = 0.06) on PFK protein content (Fig. 7*C*). With respect to LDH, there was a significant main effect of diet on LDH protein content in both the BRCA1KO^{smi} and WT mice, but no effect of genotype (P = 0.065) on LDH protein content (Fig. 7*D*).

BRCA1KO^{smi} have altered IMLC and malonyl Co-A content compared to age-matched WT animals

Using cultured human myocytes, we previously reported that decreased Brca1 expression resulted in higher lipid droplet content and reduced acetyl CoA carboxylase activity (5). In the mice, we assessed total lipid droplet content within skeletal muscle fibers by assessing cross-sections of the TA muscle using the neutral lipid stain, BODIPY (**Fig. 8*A***). A significant main effect of lipid droplet content was detected for both diet and genotype (Fig. 8A). Specifically, animals consuming an HFD exhibited elevated lipid droplet content,

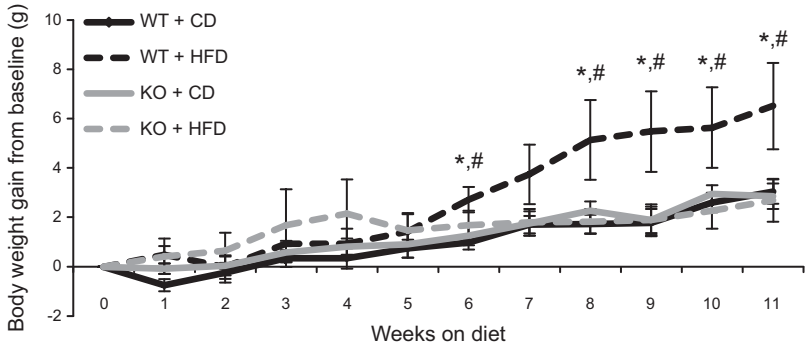

Figure 3. Loss of functional Brca1 in skeletal muscle prevents HFD-induced increases in body weight. WT and BRCA1KO^{smi} mice were fed a CD or an HFD for 10 wk. After 6 wk of the diet, WT-HFD mice had significantly greater body mass than did WT-CD and BRCA1KO^{smi}-HFD mice (n = 7–10 mice/group). Means ± SEM. *$P \leq 0.05$, WT-HFD *vs.* WT-CD; #$P \leq 0.05$, WT-HFD *vs.* BRCA1KO^{smi}-HFD.

TABLE 1. *Average food consumption of each genotype per day*

Genotype	Food consumption (g/d)	SEM	Food consumption (kcal/d)	SEM
WT-CD	3.4	0.2	13	0.7
WT-HFD	3.1	0.2	14.9	0.8
KO-CD	3.9*	0.3	15.2*	1.3
KO-HFD	3.5*	0.1	16.5*	0.7

*Main effect of genotype. $P < 0.05$ (n = 6–10 animals/group).

whereas the BRCA1KO^{smi} mice had significantly less lipid droplet content compared to the WT groups. Within groups, lipid droplet content was greater in WT-HFD mice compared with WT-CD and BRCA1KO^{smi}-HFD mice. Similarly, IMLC in BRCA1KO^{smi}-HFD mice was greater than KO-CD. Confirming our previous *in vitro* results, we found a significant main effect of genotype *in vivo*, with a ~56% lower malonyl CoA content in the KO mice *vs.* the WT group (Fig. 8*B*). No effect of diet was detected.

BRCA1KO^{smi} exhibit reduced rates of mitochondrial respiration compared to that in age-matched WT animals

Previous work in nonmuscle tissue has implied that Brca1 protein can localize to the mitochondria; however, it is unclear whether Brca1 influences the respiration kinetics of the mitochondria. In these experiments, mitochondrial respiration was assessed using the isolated mitochondria from animals' muscles in each group. No significant differences (P = 0.08) were detected in basal complex I (malate/glutamate, No ADP)–induced respiration in BRCA1KO^{smi} mice compared to WT (**Fig. 9*A***). However, a significant main effect was detected in state 3 respiration (malate/glutamate, with ADP) in BRCA1KO^{smi} mice compared to WT (Fig. 9*A, B*). Furthermore, under basal- and ADP-stimulated conditions, the exposure of the WT or the BRCA1KO^{smi} group to the HFD did not further reduce mitochondrial respiration rates (Fig. 9*A, B*). The mitochondria isolated from BRCA1-KO^{smi} mice fed a CD demonstrated minimal changes in mitochondrial complex content (Fig. 9*C*). Exposure of the BRCA1KO^{smi} mice to an HFD resulted in all of the mitochondrial complexes being significantly lower than in the WT-CD group, whereas the WT-HFD group demonstrated only lower complex I and II content compared to the WT-CD group. To ensure no off-target effects developed due to the tamoxifen exposure, we performed the same tamoxifen injection procedure on Cre^{+}-only animals or in Brca (fl/fl)-only animals. We then performed skeletal muscle mitochondrial respiration experiments in the same fashion as described in Materials and Methods. We found no differences in basal (P = 0.43) or ADP (P = 0.72) stimulated respiration when comparing animals treated with tamoxifen compared to vehicle-treated animals (data not shown).

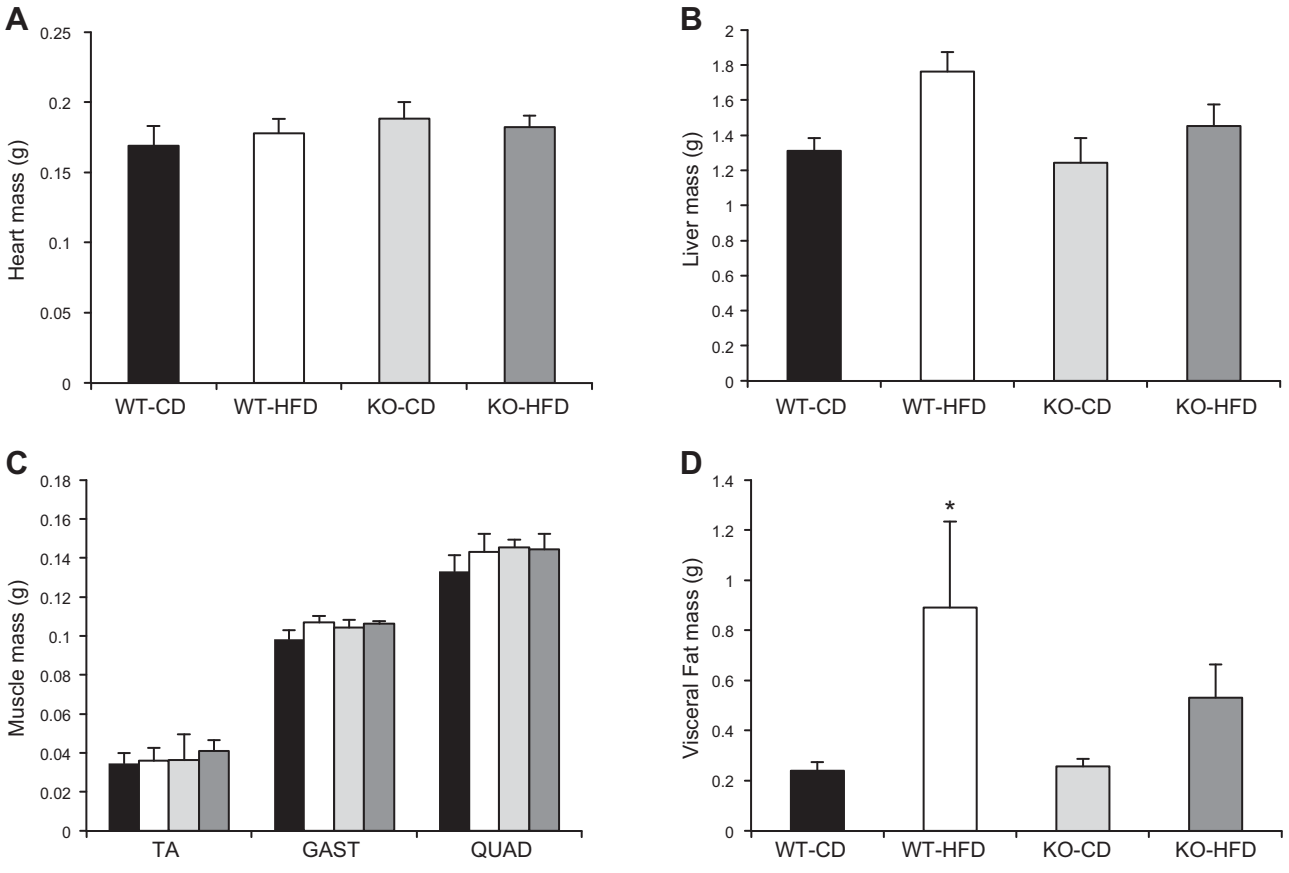

Figure 4. Loss of Brca1 expression in skeletal muscle does not affect organ tissue mass, regardless of diet. WT and BRCA1KO^{smi} mice were placed on a CD or an HFD for 10 wk. Heart mass (*A*), liver mass (*B*), skeletal muscle mass (TA; GAST, gastrocnemius; and QUAD, quadriceps) (*C*), and visceral adipose tissue mass (*D*). After 10 wk of HFD feeding, WT-HFD mice had significantly greater visceral fat mass compared to WT-CD (n = 7–10 mice/group). Means ± SEM. *$P \leq 0.05$.

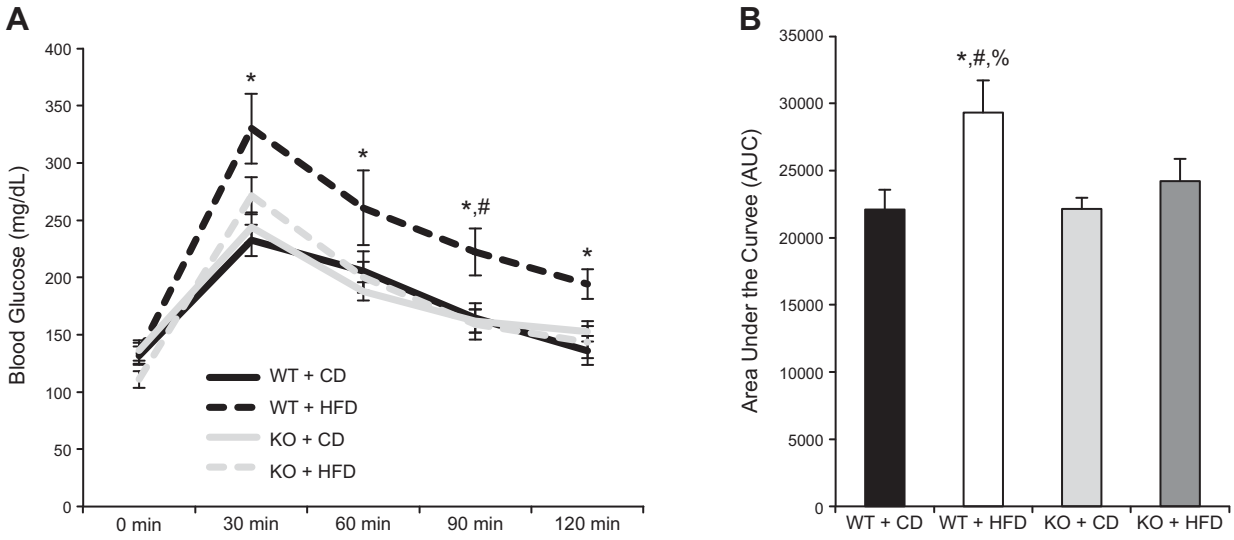

Figure 5. Deletion of Brca1 in skeletal muscle prevents HFD-induced glucose intolerance. *A*) No significant differences in blood glucose levels were detected across groups at baseline. After a glucose injection, blood glucose levels were higher in WT-HFD mice than in WT-CD mice at 30, 60, 90, and 120 min. $^{*}P \leq 0.05$. WT-HFD blood glucose levels were greater than BRCA1KO^{smi}-HFD at 90 min after glucose injection. $^{\#}P \leq 0.05$. *B*) Total area under the curve was greater in WT-HFD mice than WT-CD mice, BRCA1KOsmi-CD mice, or BRCA1KOsmi-HFD mice (n = 6–10 mice/group). $^{*}P \leq 0.05$, WT-HFD *vs.* WT-CD; $^{\%}P \leq 0.05$ WT-HFD *vs.* BRCA1KOsmi-CD; $^{\#}P \leq 0.05$ WT-HFD *vs.* BRCA1KOsmi-HFD mice. No significant differences were detected between WT-CD and BRCA1KO^{smi}-CD mice.

Electron microscopy demonstrates that BRCA1KO^{smi} mice have enlarged mitochondria compared to those in age-matched WT animals

Based on the mitochondrial respiration results, we captured red gastrocnemius muscles from another cohort of animals exposed to CD to visualize muscle ultrastructure. Using CD-diet-only animals was justified, because there was no diet effect on the mitochondrial respiration data. The EM imaging demonstrated enlarged mitochondria throughout the muscle in the BRCA1KO^{smi} mice compared to the muscle in the age-matched WT animals (**Fig. 10**).

Skeletal muscle from BRCA1KO^{smi} mice do not exhibit alterations in content of key regulatory proteins of mitochondrial fission, compared with that in age-matched WT animals

Our respiration data and electron microscopy imaging of the mitochondria suggest that deletion of BRCA1 from

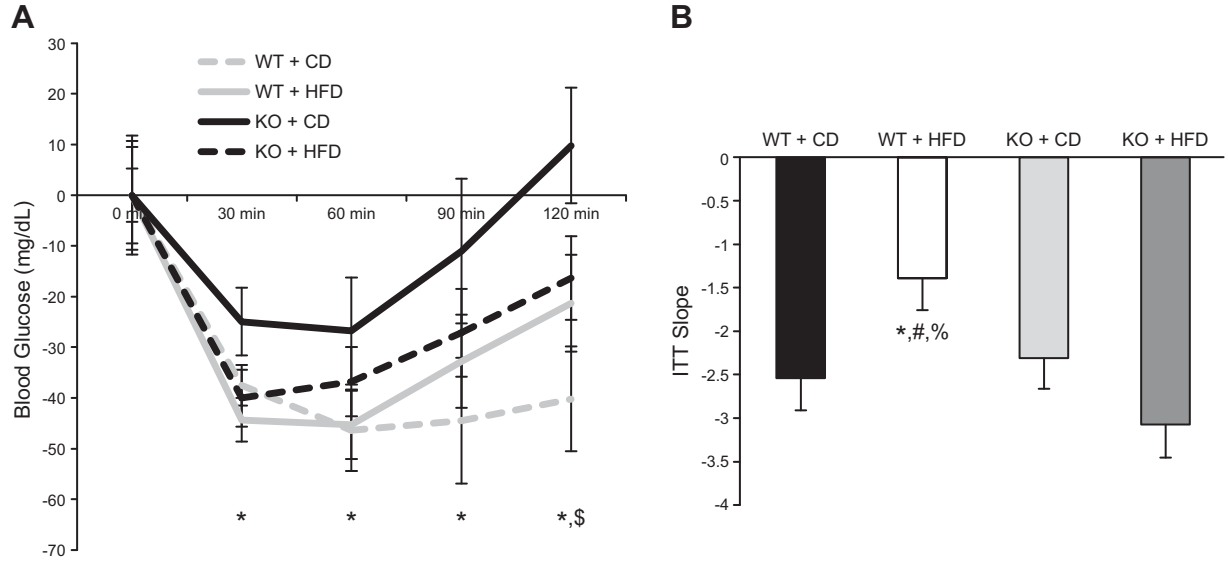

Figure 6. Deletion of Brca1 in skeletal muscle prevents HFD-induced insulin intolerance. *A*) No significant differences in blood glucose levels were detected across groups at baseline. After an IP insulin injection, blood glucose levels were higher in WT-HFD mice than in WT-CD mice at 30, 60, 90 and 120 min. $^{*}P \leq 0.05$. There was a main effect of genotype at 120 min after glucose injection. $^{\$}P \leq 0.05$. *B*) Slope from 0 to 30 min after insulin injection was reduced in WT-HFD mice compared with WT-CD mice, BRCA1KO^{smi}-CD mice, and BRCA1KO^{smi}-HFD mice (n = 6–10 mice/group). $^{*}P \leq 0.05$, WT-HFD *vs.* WT-CD; $^{\%}P \leq 0.05$, WT-HFD *vs.* BRCA1KO^{smi}-CD; $^{\#}P \leq 0.05$, WT-HFD *vs.* BRCA1KO^{smi}-HFD.

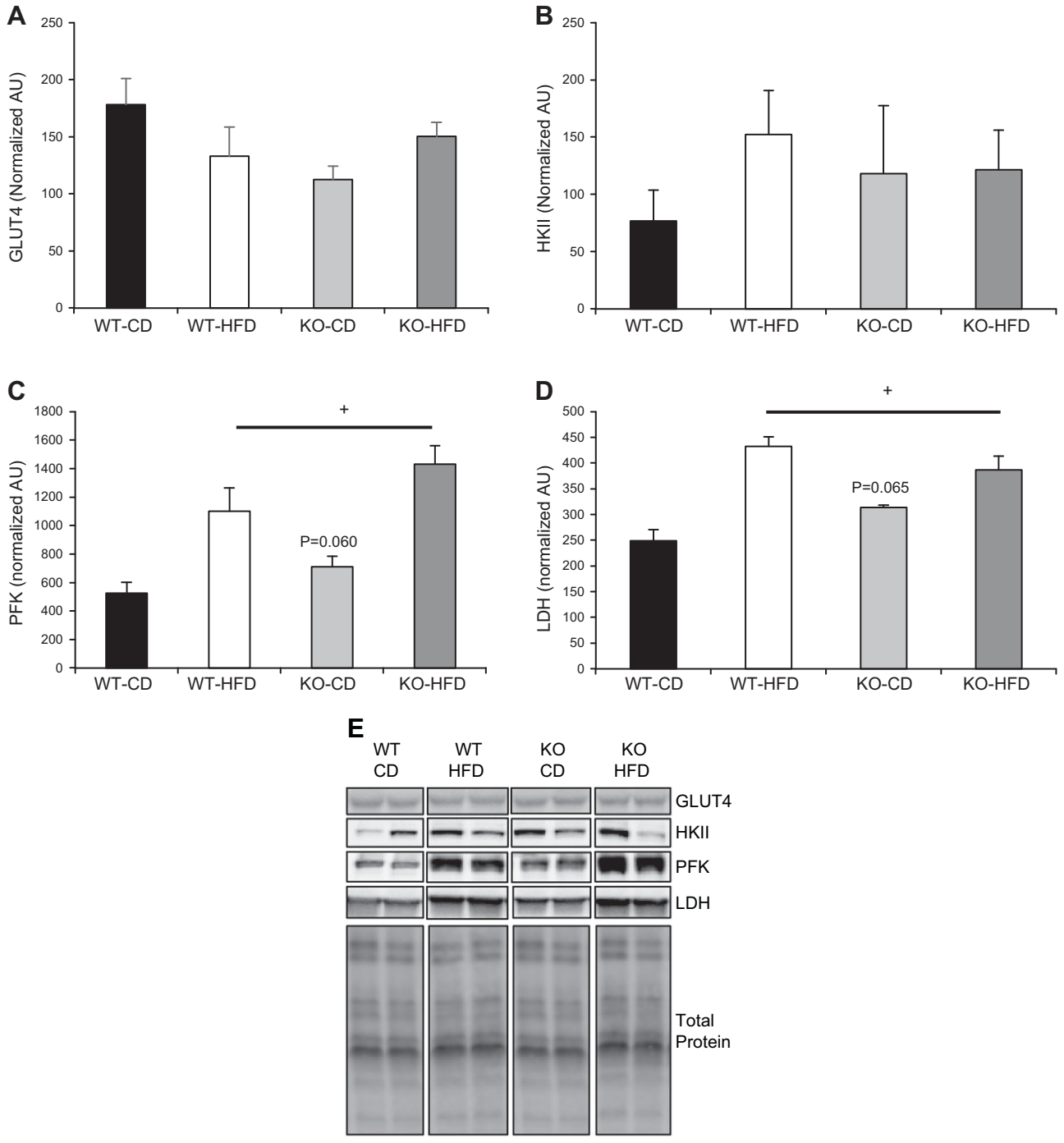

Figure 7. Protein content of GLUT4 and glycolytic enzymes in skeletal muscle from age-matched WT and BRCA1KO^{smi} mice. *A*) No significant differences were detected in GLUT4 protein content in the TA muscle from age matched WT and BRCA1KO^{smi} mice that were fed the CD or HFD. *B*) No significant differences were detected in HKII protein content in the TA muscle from age-matched WT and BRCA1KO^{smi} mice exposed to the CD or HFD. *C*) PFK protein content was elevated in WT and KO mice fed an HFD. +, Main effect of diet, $P \leq 0.05$. *C*) WT-CD *vs.* KO-CD. $P < 0.06$ (no significant difference). *D*) LDH protein content was higher in WT and KO mice fed an HFD. +, Main effect of diet, $P \leq 0.05$. WT-CD *vs.* KO-CD almost reached statistical significance. ($n = 4$–6 mice/group). $P = 0.065$. *E*) Examples of bands measured from the Western blots from each target in each group. Please note that noncontiguous bands are shown in the examples.

skeletal muscle would result in an inability to remove swollen, compromised mitochondria from the muscle cell. To test this notion, we measured the phosphorylation and total protein content of 2 key regulators of pathways that affect the quality control of the mitochondria, the ubiquitin E3-ligase Parkin, and dynamin-related protein (Drp)-1. Parkin is known to affect mitophagy, thus affecting clearance rates of mitochondria, whereas Drp1 promotes mitochondrial fission activity. We found a main effect of diet on the phosphorylation of Parkin and Drp1 in both genotypes of mice, with no effect of genotypes on either phosphorylation event (**Fig. 11**).

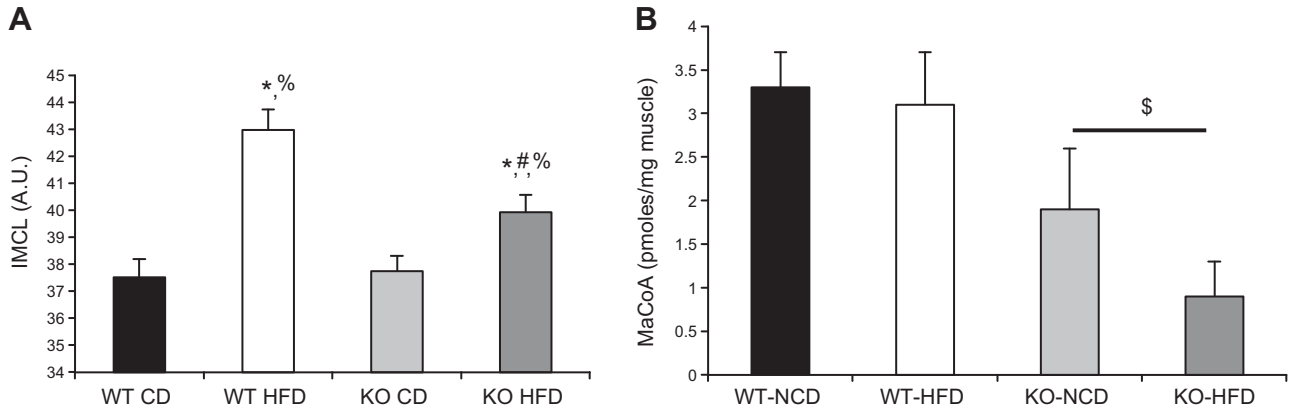

Figure 8. HFD-induced IMLC accumulation is attenuated in response to loss of Brca1 in skeletal muscle. *A*) Lipid droplet content was significantly elevated in the TA muscle in both the WT- and BRCA1KO^{smi}-HFD mice compared with the WT- and BRCA1KO^{smi}-CD mice. BRCA1KO^{smi}-HFD IMLC accumulation was lower than that in WT-HFD. Means ± SEM. *$P \leq 0.05$ *vs.* WT-CD; $^{\%}P \leq 0.05$ *vs.* BRCA1KO^{smi}-CD; and $^{\#}P \leq 0.05$ *vs.* BRCA1KO^{smi}-HFD. *B*) BRCA1KO^{smi} exhibited decreased skeletal muscle malonyl Co-A content compared with the WT groups. HFD had no effect on malonyl Co-A content in either genotype (n = 5–6 mice/group). $^{\$}P \leq 0.05$ *vs.* both WT groups.

BRCA1 localizes to the mitochondria in skeletal muscle

To assess Brca1 localization in skeletal muscle, a previously established somatic gene delivery approach was used (16). The assessment of endogenous murine Brca1 localization through antibody labeling is not feasible because of the poor reliability of murine-specific Brca1 antibodies. However, previous groups have shown that Brca1-YFP constructs replicate functional characteristics of endogenous Brca1 (9, 17). Using full-length BRCA1-YFP cDNA (**Fig. 12*A***, pseudocolored green) or YFP only (data not shown), we electroporated each construct into the FDB muscle and then isolated single muscle fibers. The Brca1-YFP showed a distinct localization pattern throughout the muscle fiber, whereas YFP only exhibited a diffuse signal (data not shown). To identify compartments of Brca1-YFP localization, the muscle myonuclei (blue) and mitochondria (red, Fig. 12*B*) were stained. Brca1-YFP localized to multiple areas of the muscle fiber including nuclei, mitochondria, and other cytosolic compartments. Specifically, using Mander's coefficient calculations (**Table 2**), we found that Brca1-YFP localizes within the nucleus and the mitochondria in adult skeletal muscle cells.

BRCA1KO^{smi} mice exhibit increased V_{CO_2}, RER and energy expenditure

We have demonstrated that the BRCA1KO^{smi} mice consumed more kilocalories (independent of diet) without gaining weight, which was associated with reduced mitochondrial respiration in the KO *vs.* the WT mice. These results suggest that loss of Brca1 expression in skeletal muscle leads to reduced mitochondrial efficiency. To test this concept, we used a second cohort of mice and assessed whole-body indirect calorimetry of age-matched WT and KO mice. Because KO mice consumed more food and exhibited reduced mitochondrial respiration regardless of diet, only the CD diet was used. We found no differences in V_{O_2} consumption between groups (**Fig. 13*A***). However, the BRCA1KO^{smi} mice exhibited increased whole-body V_{CO_2}, increased RER, and increased energy expenditure during the dark cycle when compared to those parameters in the age-matched WT mice (Fig. 13*B*–*D*).

BRCA1KO^{smi} mice have reduced exercise tolerance *vs.* age-matched WT mice

Using a well-established rodent treadmill protocol, we found a significant main effect of genotype in that the BRCA1KO^{smi} exhibited reducing running speeds and distances compared with those in the WT mice (**Fig. 14**). We also found that consuming the HFD resulted in a main-effect of reduced running speeds and distances regardless of genotype; however there was no additive effect of diet in the KO mice.

DISCUSSION

Using *in vitro* models, we had identified Brca1 as a novel regulator of metabolic function in skeletal muscle (5). In the current study, using an *in vivo*–based approach, we extended our previous results by demonstrating that induced loss of Brca1 in the skeletal muscle of adult mice results in reduced ADP-stimulated complex I–driven mitochondrial respiration and enlarged mitochondrial size. We also determined that Brca1 is capable of localizing to mitochondria as well as the nuclei in skeletal muscle cells. Using an exercise tolerance test, we found functional deficits in the BRCA1KO^{smi} when compared to the WT animals. When compared to the WT mice fed an HFD, exposure of the BRCA1KO^{smi} to an HFD failed to elicit similar gains in body weight and changes in insulin response and glucose tolerance. We attribute the lack of a dietary effect on BRCA1KO^{smi} to increased whole-body energy expenditure and differences in mitochondrial

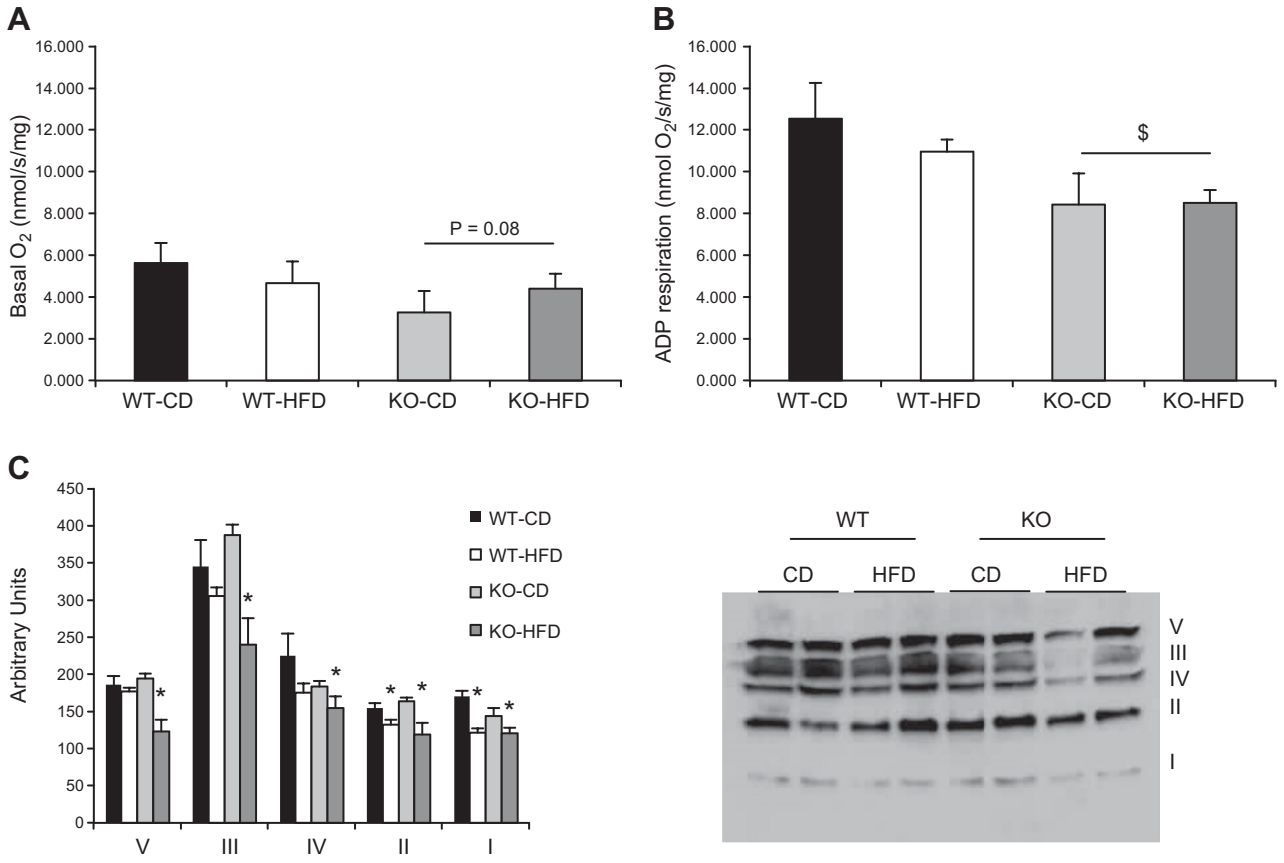

Figure 9. Deletion of Brca1 in skeletal muscle results in reduced ADP-stimulated mitochondrial respiration in skeletal muscle. *A*) Basal O_2 consumption was assessed in isolated mitochondria from quadriceps muscles of animals in each group after malate/glutamate delivery without ADP. There was a trend toward a main effect of genotype. $P = 0.08$, KO *vs.* WT. *B*) A main effect of genotype was detected in ADP stimulated respiration rates when comparing the BRCA1KO^{smi} to the WT groups. Means ± SEM. $^{\$}P \leq 0.05$. ADP respiration is the O_2 consumption rate after 300 μM ADP delivery. *C*). BRCA1KO^{smi} mice consuming the CD showed minimal alterations in specific complex content with the exception of complex I in the isolated mitochondria compared to the WT animals. In contrast, BRCA1KO^{smi} mice fed an HFD showed significant decreases in content of all the complexes compared to the WT-CD mice ($n = 5$ mice/group).

efficiency between BRCA1KO^{smi} and WT mice. Our data suggest that deletion of Brca1 in mouse skeletal muscle induces mitochondrial inefficiencies that allow mice to simultaneously increase food intake while attenuating weight gain. Overall, the findings clearly demonstrate that induced loss of Brca1, specifically in skeletal muscle, leads to a complex and multifaceted metabolic phenotype.

BRCA1KO^{smi} mice exhibited reductions in skeletal muscle mitochondrial respiration compared with the WT mice, regardless of diet. Specifically, isolated mitochondria from the BRCA1KO^{smi} mice exhibited reduced rates of complex I–stimulated respiration in ADP-driven conditions when compared to the WT group. In nonmuscle tissue, modulation of Brca1 expression can alter oxidative metabolism by reducing catabolism of palmitate, whereas conditional deletion of Brca1 in cardiac tissue results in decreased glucose and palmitate oxidation (4). Thus, when assessed collectively across various cell types, the data support the notion that Brca1 expression is necessary for maintenance of multiple aspects of mitochondrial function.

Brca1 overexpression in cultured breast cancer cells resulted in the reduction of glycolytic gene expression and enhanced mitochondrial gene expression (6). However, we found only minor changes in protein content of each mitochondrial complex, which is surprising, considering the differences in the mitochondrial morphology in the BRCA1KO^{smi} mice. Further, we did not detect significant changes in the protein content of various enzymes in glycolysis, albeit a limitation of this study is that we cannot confirm that the activities of these glycolytic enzymes did not change. The underlying mechanisms explaining how Brca1 influences mitochondrial function are largely unknown, but our data suggest that Brca1 can localize to the mitochondria in a fashion similar to that observed in MCF7 breast carcinoma cells, suggesting that Brca1 can directly influence the mitochondria (8, 9). It remains unclear how Brca1 locates to the mitochondria, because Brca1 does not contain a consensus mitochondrial localization sequence. A likely possibility is that the Brca1 protein is piggybacking into the mitochondria through an interaction with another protein that contains a mitochondrial localization sequence (17). In fact, a similar mechanism was discovered for Brca1 movement into the nucleus (17); however not all studies support our finding that Brca1 localizes in the mitochondria (21). These

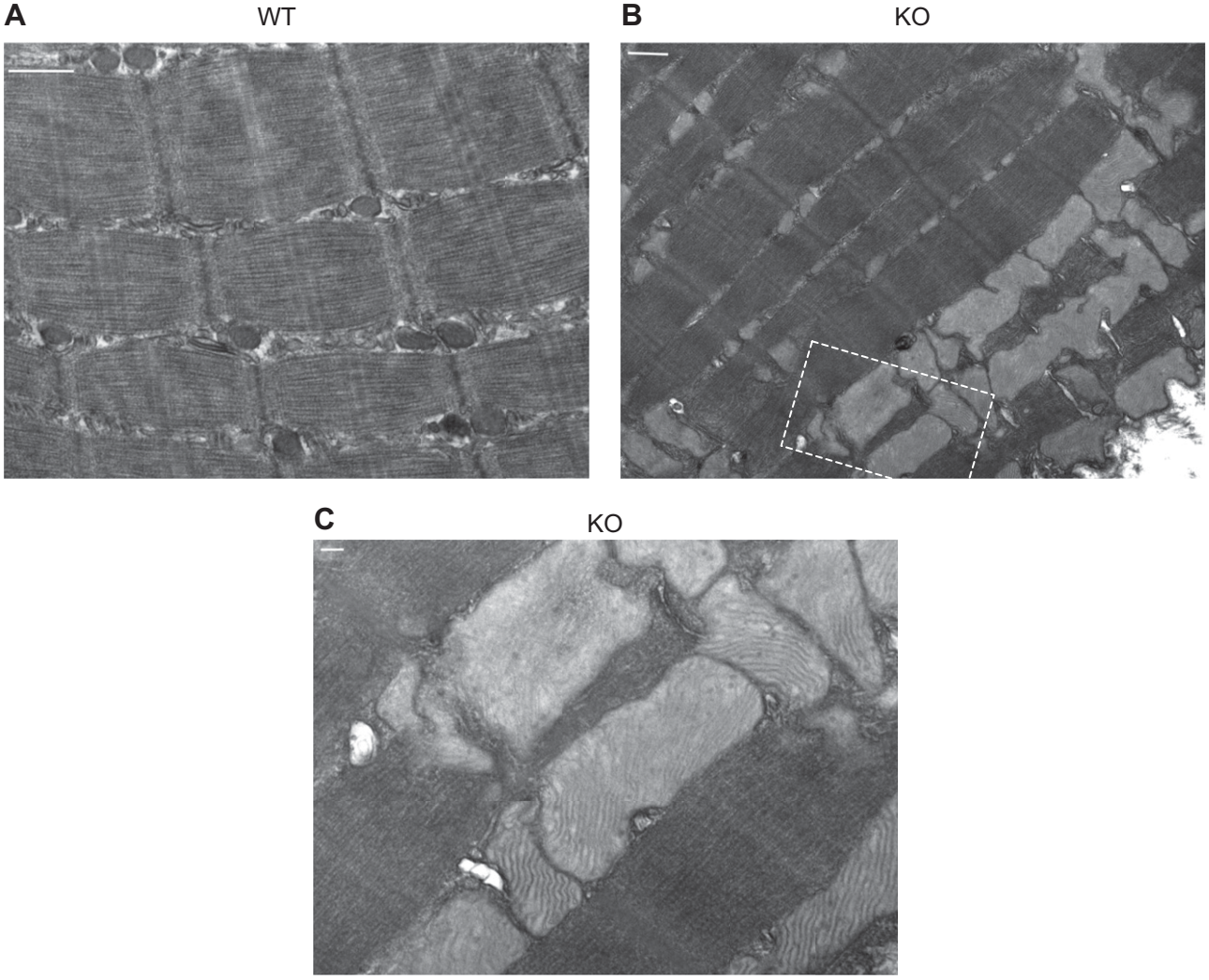

Figure 10. Deletion of Brca1 results in dilated skeletal muscle mitochondria compared to aged-matched WT mice. Representative electron micrographs of deep gastrocnemius muscles demonstrate enlarged mitochondria in KO *vs.* WT mice. *A*) Normal muscle ultrastructure in red gastrocnemius muscle from WT male mice. Scale bar, 500 nm. *B*) Muscle ultrastructure imaged in red gastrocnemius muscle of age-matched male mouse KO red gastrocnemius muscle. Scale bar, 500 nm. *C*) High-magnification image (taken from area within the box in image *B*). Scale bar, 100 nm.

differences across studies may, in part, be related to the dependency on Brca1 antibodies that lack precise antigen-binding characteristics with endogenous Brca1. Alternatively, the varying results could be because Brca1 has different localization patterns depending upon the tissue type under experimental consideration.

BRCA1KO^{smi} mice exhibited normal glucose tolerance and no additive weight gain when exposed to an HFD compared to age-matched WT mice on the same HFD. These data suggest that loss of Brca1 attenuates the negative metabolic responses commonly associated with HFD consumption. Although the protection of the BRCA1-KO^{smi} mice from an HFD is surprising when considering the reduction in mitochondrial respiration, there is precedence for similar results in animal models. For example, the POLG mutator mice exhibit significant losses in oxidative capacity related to the loss of a mitochondrial DNA proofreading enzyme, but remained protected from the deleterious effects of an HFD because of higher glycolytic capacities (22). A recent review of the literature found several examples of mouse models that demonstrated metabolic protection from an HFD (23), with many of the mouse models that demonstrated metabolic protection exhibiting decreases in mitochondrial respiration. Altogether, this suggests that, temporarily, an animal can adapt to exposure to nutrient overload by altering the metabolic (*i.e.*, glycolytic) phenotype of the skeletal muscle tissue. In support of this hypothesis, the BRCA1KO^{smi} mice exhibited increased RER and energy expenditure during the dark cycle, suggesting that the mice were catabolizing more carbohydrate while expending an increased amount of energy compared with the WT mice. Thus, the findings suggest that deletion of exon 11 in the *Brca1* gene leads to changes in the metabolic phenotype of the skeletal muscle; however, more comprehensive studies are needed to determine whether alterations in glucose utilization develop in the BRCA1KO^{smi} mice. Our data add to accumulating evidence suggesting that decreases in mitochondrial respiratory capacity do not

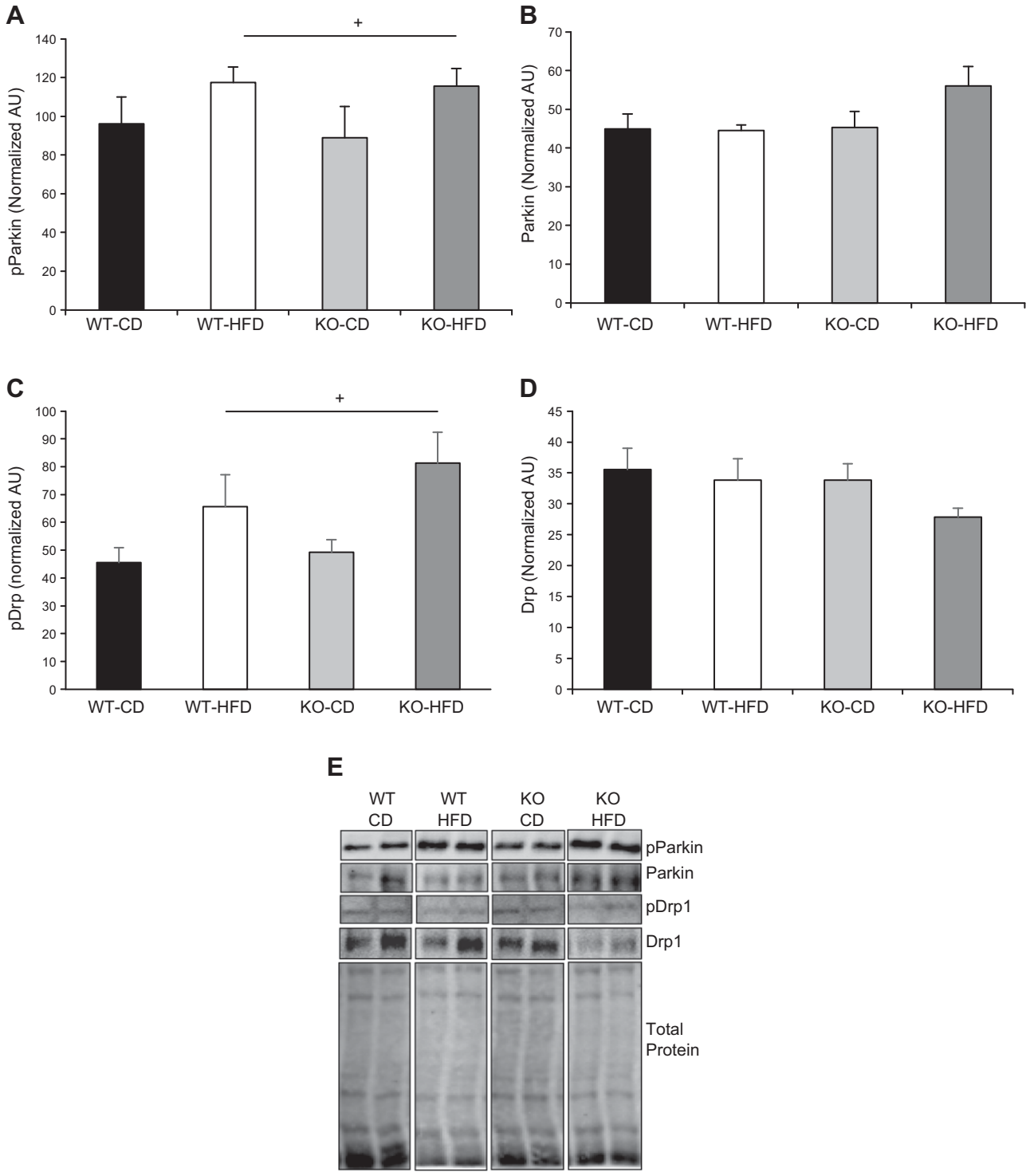

Figure 11. Loss of BRCA1 does not affect Parkin or Drp1 phosphorylation in skeletal muscle. *A*, *B*) No significant differences were detected in GLUT4 protein content in the TA muscle from age-matched WT and BRCA1KO^{smi} mice that were fed normal CD or HFD. *B*) No significant differences were detected in HKII protein content in the TA muscle from age-matched WT and BRCA1KO^{smi} mice that were fed a CD or an HFD. *C*) PFK protein content was elevated in WT and KO exposed to an HFD. +, Main effect of diet, $P \leq 0.05$. WT-CD *vs.* KO-CD exhibited a trend toward statistical significance. $P = 0.060$. *D*) LDH protein content was higher in WT and KO fed to an HFD. +, Main effect of diet. $P \leq 0.05$. WT-CD *vs.* KO-CD almost reached statistical significance ($n = 4$–6 mice/group). $P = 0.065$. *E*) Examples of bands measured from the Western blots from each target in each group. Noncontiguous bands are shown in the examples.

necessarily correspond with increased susceptibility to glucose intolerance in HFD conditions.

The *in vivo* effects of Brca1 loss in skeletal muscle are in contrast to some of our previous findings where we induced acute decreases in *BRCA1* expression using an shRNA based approach in cultured human myotubes (5). In cultured human myotubes, we found that reductions in *BRCA1* mRNA led to reduced insulin signaling and lower

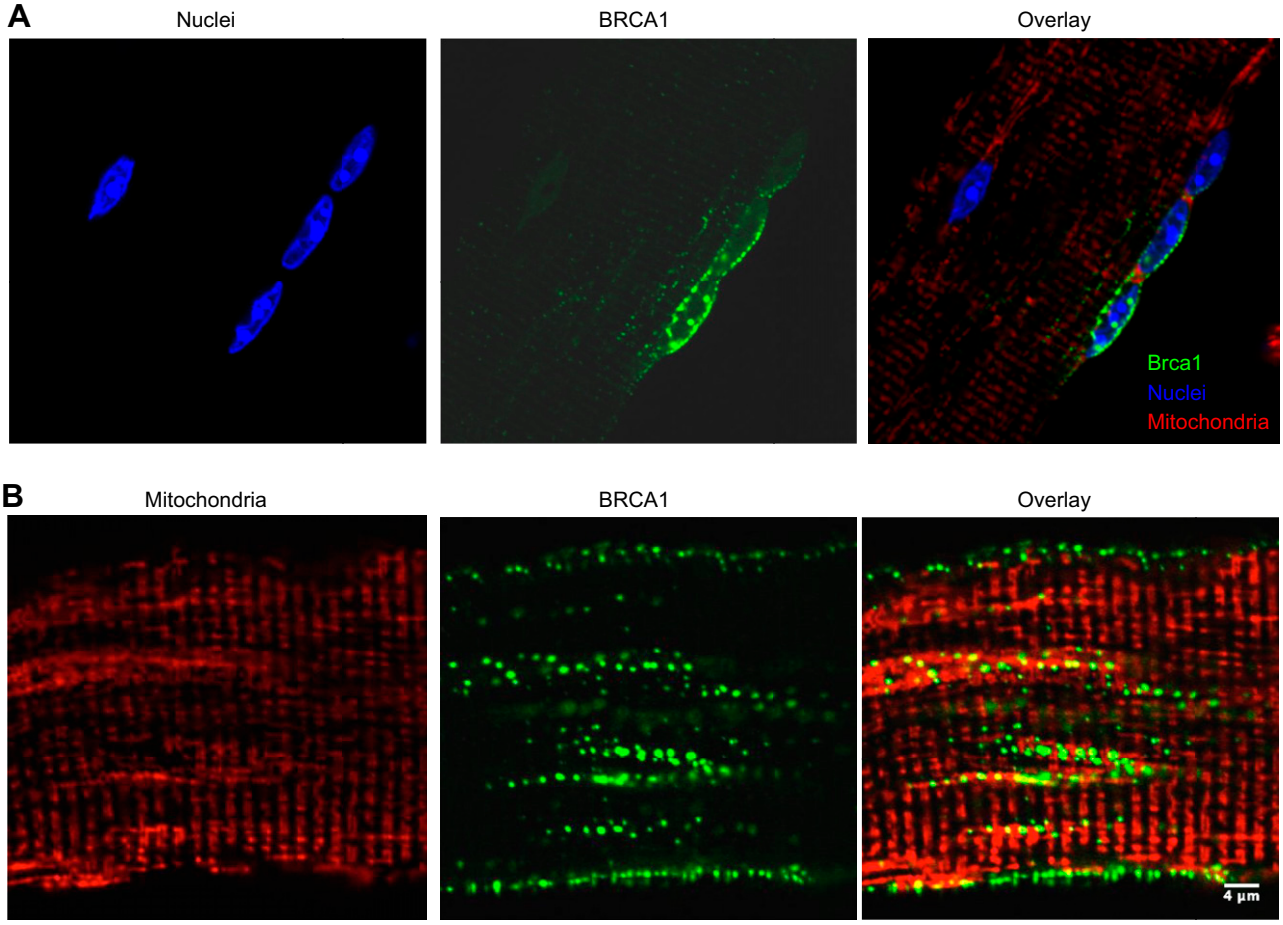

Figure 12. BRCA1 localizes to the mitochondria and nucleus in skeletal muscle cells. Sample images of BRCA1-YFP (pseudocolored green)-positive single muscle fibers isolated from the FDB muscle after the fibers were stained for DAPI (blue) and mitochondria (red). BRCA1-YFP signal localized to specific areas of the cell. *A*) BRCA1-YFP and nucleus, entire cell outlined in white. *B*) BRCA1-YFP and mitochondria (red). Brca1-YFP exhibited discrete patterns of expression that appeared only in some mitochondria and some nuclei of each visualized muscle cell. Mander's coefficient calculations were determined between BRCA-1-YFP and red tracker DS signal and BRCA-1-YFP and DAPI signal (Table 2). Muscle fibers positive only for YFP did not show the same localization as the BRCA1-YFP plasmid (data not shown). BRCA1-YFP localization was assessed in 20+ muscle fibers. Scale bar, 4 µm.

insulin-induced glucose uptake. The results may have differed for several reasons. First, it is possible there are differential consequences of acute *vs.* chronic loss of Brca1 and our data represent an adaptation response from prolonged *in vivo* loss of Brca1 in the mouse model. Second, the human myotube culture model does not completely replicate the *in vivo* environment leading to a difference in response to Brca1 deletion. Third, it is plausible that deletion of Brca1 in mice leads to different metabolic responses compared with that in human tissue. Regardless of the reason, loss of BRCA1 in human myotubes and in skeletal muscle from BRCA1KO^{smi} mice results in reduced mitochondrial respiration, suggesting that Brca1 is important for mitochondrial function in skeletal muscle.

BRCA1 missense mutations resulting in partial or complete deletion of Brca1 occur in humans, but there is little to no information reported regarding the physiologic consequences of these mutations. Although *BRCA1* mutations in women are frequently associated with an increased risk of tumorigenesis, our data suggested that skeletal muscle function is also altered. For example, individuals with *BRCA1* mutations may have reduced mitochondrial respiration or alterations in skeletal muscle metabolic function or both; however, this has not been empirically tested. The growing number of reports regarding changes in skeletal muscle, coupled with evidence in the brain and cardiovascular system (2, 3), suggest a role for Brca1 function in tissues outside of the mammary gland. Considering the vast number of mutations in the *BRCA1* gene, it is critical that more studies be pursued to address Brca1 function to identify possible cellular mechanisms regulated by the protein.

In summary, our data demonstrate for the first time that Brca1 localizes to the mitochondria in skeletal

TABLE 2. *Colocalization of BRCA1-YFP with nucleus or mitochondria*

Statistic	Nucleus, YFP/DAPI	Mitochondria, YFP/MTDR
Mander's coefficient	0.426 ± 0.06	0.262 ± 0.02

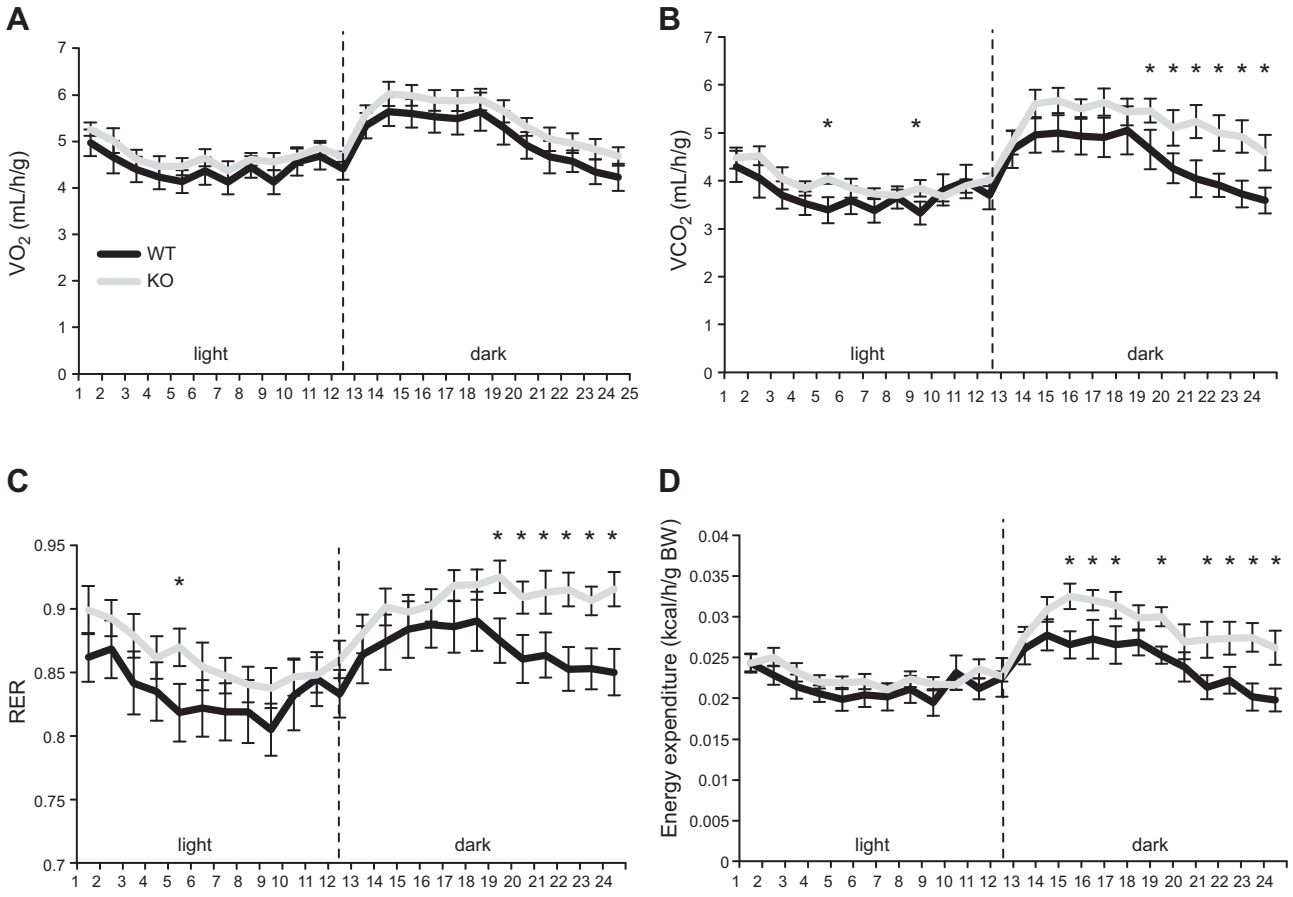

Figure 13. Ablation of Brca1 in skeletal muscle increases whole body metabolic activity. Age-matched BRCA1KO^{smi} and WT mice were individually housed in metabolic cages for 5 d. The first 2 d were used to acclimate the mice to the cages, with the data representing the mean data collected over the final 3 d (n = 8–12/group). Mean whole-body Vo_2 (*A*); Vco_2 (*B*); RER (Vco_2/Vo_2) (C); and energy expenditure according to body weight (*D*). Means ± SEM (n = 6–10 mice/group). *$P < 0.05$, WT *vs.* KO.

muscle and that expression of Brca1 is critical for maintenance of mitochondrial respiration. Deletion of Brca1 protects mice from developing the metabolic consequences commonly associated with an HFD. Future experiments to assess the impact of known Brca1 mutations on mitochondrial and metabolic function are critical for providing new knowledge to individuals with *BRCA1* mutations. FJ

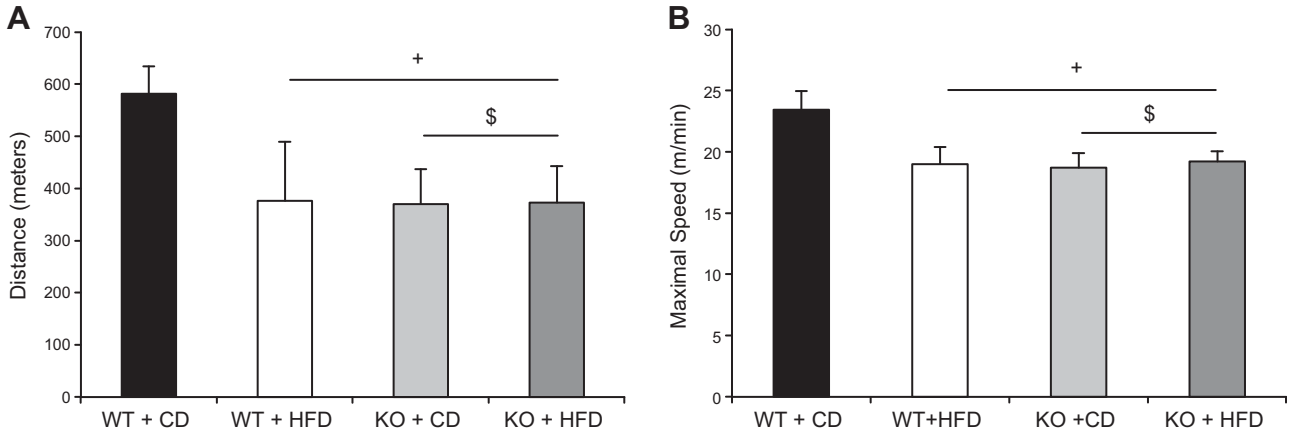

Figure 14. Exercise tolerance is reduced with ablation of Brca1 in skeletal muscle. BRCA1KO^{smi} mice exhibited reduced running distances (*A*) and running speeds (*B*) compared to age-matched WT mice. Age-matched BRCA1KO^{smi} and WT mice were acclimated to the treadmill, and then each mouse performed an acute exercise bout after completion of the acclimation period. A main effect of genotype and diet was detected in when comparing the BRCA1KO^{smi} with the WT groups. Means ± SEM (n = 6–8 mice/group). $^{+}P \leq 0.05$ *vs.* WT-CD; $^{\$}$ $P \leq 0.05$, KO-CD *vs.* KO-HFD.

ACKNOWLEDGMENTS

The authors thank Tom Greene (East Carolina University, Greenville, NC, USA) for technical assistance; BRCA1 plasmids were kind gift of Dr. B. Henderson (Westmead Institute for Cancer Research, Sydney, NSW Australia), and Dr. John McCarthy (University of Kentucky, Lexington, KY, USA) for numerous helpful discussions concerning animal breeding. This work was funded U.S. National Institutes of Health (NIH), National Institute of Arthritis and Musculoskeletal and Skin Diseases Grants R21AR059913, RO1AR066660, R01AR059179, and R21AR067872 (to R.M.L.); NIH National Heart, Lung, and Blood Institute Grant RO1HL125695 (to J.M.M.); and NIH National Institute on Aging Grant T32 AG000268 (to K.C.J. and A.P.V.). The authors declare no conflicts of interest.

AUTHORS CONTRIBUTIONS

K. C. Jackson designed the research, analyzed the data, performed the research, and wrote the paper; A. P. Valencia, M. R. Iñigo, and M. D. Tarpey designed the research, analyzed the data, and performed the research; E. E. Spangenburg analyzed data and wrote the paper; S. J. Pratt, D. J. Patteson, and D. M. Thomson analyzed the data and performed the research; and J. M. McClung and R. M. Lovering designed the research and contributed analytic tools.

REFERENCES

1. Roy, R., Chun, J., and Powell, S. N. (2011) BRCA1 and BRCA2: different roles in a common pathway of genome protection. *Nat. Rev. Cancer* **12**, 68–78
2. Pao, G. M., Zhu, Q., Perez-Garcia, C. G., Chou, S.-J., Suh, H., Gage, F. H., O'Leary, D. D. M., and Verma, I. M. (2014) Role of BRCA1 in brain development. *Proc. Natl. Acad. Sci. USA* **111**, E1240–E1248
3. Suberbielle, E., Djukic, B., Evans, M., Kim, D. H., Taneja, P., Wang, X., Finucane, M., Knox, J., Ho, K., Devidze, N., Masliah, E., and Mucke, L. (2015) DNA repair factor BRCA1 depletion occurs in Alzheimer brains and impairs cognitive function in mice. *Nat. Commun.* **6**, 8897
4. Lovren, F., Pan, Y., Quan, A., Singh, K. K., Khan, R., Gupta, N., Brezden-Masley, C., Teoh, H., Wheatcroft, M. D., Al-Omran, M., and Verma, S. (2014) BRCA1 shields vascular smooth muscle cells from oxidative stress. *J. Thorac. Cardiovasc. Surg.* **147**, 1946–1955.e1
5. Jackson, K. C., Gidlund, E. K., Norrbom, J., Valencia, A. P., Thomson, D. M., Schuh, R. A., Neufer, P. D., and Spangenburg, E. E. (2014) BRCA1 is a novel regulator of metabolic function in skeletal muscle. *J. Lipid Res.* **55**, 668–680
6. Privat, M., Radosevic-Robin, N., Aubel, C., Cayre, A., Penault-Llorca, F., Marceau, G., Sapin, V., Bignon, Y. J., and Morvan, D. (2014) BRCA1 induces major energetic metabolism reprogramming in breast cancer cells. *PLoS One* **9**, e102438
7. Singh, K. K., Shukla, P. C., Yanagawa, B., Quan, A., Lovren, F., Pan, Y., Wagg, C. S., Teoh, H., Lopaschuk, G. D., and Verma, S. (2013) Regulating cardiac energy metabolism and bioenergetics by targeting the DNA damage repair protein BRCA1. *J. Thorac. Cardiovasc. Surg.* **146**, 702–709
8. Coene, E. D., Hollinshead, M. S., Waeytens, A. A., Schelfhout, V. R., Eechaute, W. P., Shaw, M. K., Van Oostveldt, P. M., and Vaux, D. J. (2005) Phosphorylated BRCA1 is predominantly located in the nucleus and mitochondria. *Mol. Biol. Cell* **16**, 997–1010
9. Maniccia, A. W., Lewis, C., Begum, N., Xu, J., Cui, J., Chipitsyna, G., Aysola, K., Reddy, V., Bhat, G., Fujimura, Y., Henderson, B., Reddy, E. S., and Rao, V. N. (2009) Mitochondrial localization, ELK-1 transcriptional regulation and growth inhibitory functions of BRCA1, BRCA1a, and BRCA1b proteins. *J. Cell. Physiol.* **219**, 634–641
10. McCarthy, J. J., Srikuea, R., Kirby, T. J., Peterson, C. A., and Esser, K. A. (2012) Inducible Cre transgenic mouse strain for skeletal muscle-specific gene targeting. *Skelet. Muscle* **2**, 8
11. Xu, X., Wagner, K. U., Larson, D., Weaver, Z., Li, C., Ried, T., Hennighausen, L., Wynshaw-Boris, A., and Deng, C. X. (1999) Conditional mutation of Brca1 in mammary epithelial cells results in blunted ductal morphogenesis and tumour formation. *Nat. Genet.* **22**, 37–43
12. Garcia-Cazarin, M. L., Snider, N. N., and Andrade, F. H. (2011) Mitochondrial isolation from skeletal muscle. *J. Vis. Exp.* **49**, 2452
13. Spangenburg, E. E., Pratt, S. J. P., Wohlers, L. M., and Lovering, R. M. (2011) Use of BODIPY (493/503) to visualize intramuscular lipid droplets in skeletal muscle. *J. Biomed. Biotechnol.* **2011**, 598358
14. Wohlers, L. M., Jackson, K. C., and Spangenburg, E. E. (2011) Lipolytic signaling in response to acute exercise is altered in female mice following ovariectomy. *J. Cell. Biochem.* **112**, 3675–3684
15. Stone, M. R., O'Neill, A., Lovering, R. M., Strong, J., Resneck, W. G., Reed, P. W., Toivola, D. M., Ursitti, J. A., Omary, M. B., and Bloch, R. J. (2007) Absence of keratin 19 in mice causes skeletal myopathy with mitochondrial and sarcolemmal reorganization. *J. Cell Sci.* **120**, 3999–4008
16. DiFranco, M., Quinonez, M., Capote, J., and Vergara, J. (2009) DNA transfection of mammalian skeletal muscles using in vivo electroporation. *J. Vis. Exp.* **32**, 1520
17. Henderson, B. R. (2005) Regulation of BRCA1, BRCA2 and BARD1 intracellular trafficking. *BioEssays* **27**, 884–893
18. Dunn, K. W., Kamocka, M. M., and McDonald, J. H. (2011) A practical guide to evaluating colocalization in biological microscopy. *Am. J. Physiol. Cell Physiol.* **300**, C723–C742
19. White, A. T., LaBarge, S. A., McCurdy, C. E., and Schenk, S. (2015) Knockout of STAT3 in skeletal muscle does not prevent high-fat diet-induced insulin resistance. *Mol. Metab.* **4**, 569–575
20. Marquis, S. T., Rajan, J. V., Wynshaw-Boris, A., Xu, J., Yin, G. Y., Abel, K. J., Weber, B. L., and Chodosh, L. A. (1995) The developmental pattern of Brca1 expression implies a role in differentiation of the breast and other tissues. *Nat. Genet.* **11**, 17–26
21. Thompson, M. E. (2010) BRCA1 16 years later: nuclear import and export processes. *FEBS J.* **277**, 3072–3078
22. Wall, C. E., Whyte, J., Suh, J. M., Fan, W., Collins, B., Liddle, C., Yu, R. T., Atkins, A. R., Naviaux, J. C., Li, K., Bright, A. T., Alaynick, W. A., Downes, M., Naviaux, R. K., and Evans, R. M. (2015) High-fat diet and FGF21 cooperatively promote aerobic thermogenesis in mtDNA mutator mice. *Proc. Natl. Acad. Sci. USA* **112**, 8714–8719
23. Gilliam, L. A. A., and Neufer, P. D. (2012) Transgenic mouse models resistant to diet-induced metabolic disease: is energy balance the key? *J. Pharmacol. Exp. Ther.* **342**, 631–636

Received for publication May 19, 2017.
Accepted for publication January 2, 2018.